Measuring Temperature Distribution in Steel-Concrete Composite Slabs Subjected to Fire Using Brillouin Scattering Based Distributed Fiber Optic Sensors

Yi Bao[1], Matthew S. Hoehler[2], Christopher M. Smith[3], Matthew Bundy[2], Genda Chen[4]
[1] *Stevens Institute of Technology – USA, Email:* yi.bao@stevens.edu
[2] *National Institute of Standards and Technology - USA,* [3] *Berkshire Hathaway Specialty Insurance - USA,* [4] *Missouri University of Science and Technology - USA*

Abstract

This study investigates temperature distributions in steel-concrete composite slabs subjected to fire using distributed fiber optic sensors. Several 1.2 m × 0.9 m composite slabs instrumented with telecommunication-grade single-mode fused silica fibers were fabricated and subjected to fire for over 3 hours. Temperatures were measured at centimeter-scale spatial resolution by means of pulse pre-pumped Brillouin optical time domain analysis. The distributed fiber optic sensors operated at material temperatures higher than 900 °C with adequate sensitivity and accuracy to allow structural performance assessment, demonstrating their effective use in structural fire applications. The measured temperature distributions indicate a spatially-varying, fire-induced thermal response in steel-concrete composite slab, which can only be adequately captured using approaches that provide high data point density.

1. Introduction

The mechanical properties of construction materials and the load-carrying capacity and stability of structural members (beams, columns, slabs, and joints) are reduced at elevated temperatures (Li and Zhang 2012; Li et al. 2017a-c). To understand structural behavior during and after a fire when measured material temperature histories are unavailable, coupled thermo-mechanical analyses are often conducted (Jeffers and Sotelino 2012; Bao et al. 2016). A great number of analytical and numerical approaches have been developed to predict gas-phase temperature distributions and evolution histories resulting from fire. Zone models (Li and Zhang 2012), computational fluid dynamics models (McGrattan et al. 2010) or stochastic models (Bertola and Cafaro 2009) are often used. To date, it remains a challenge to accurately predict temperature distributions in structural members through the heat transfer analysis based on gas temperatures and radiative heat flux, in particular for structures with complex geometry, such as composite floors. The error in the predicted structural member temperature distribution and evolution over time can result in inaccurate conclusions about the mechanical response of the structure. Additionally, the uncertainty in structural element temperature distribution cannot easily be quantified.

If temperatures in structural members during a fire can be measured with fine spatial resolution, understanding the structural response due to thermal loading becomes more tractable. Traditionally in structural fire research, temperature is measured using thermocouples deployed at a limited number of discrete points. Recently, fully-distributed fiber optic sensors using pulse pre-pumped Brillouin optical time domain analysis (PPP-BOTDA) have successfully been used to measure temperature and strain in various structural applications (Bao and Chen 2016 a, b). Each instance of PPP-BOTDA can provide hundreds of temperatures measurements along the length of an optical fiber.

In this study, telecommunication-grade single-mode optical fibers are embedded in profiled concrete slabs to measure temperature distributions under fire condition. The obtained temperature data can be used to understand the structural behavior of the composite slabs.

2. Experimental Program

2.1 Specimen

The composite specimens were fabricated to develop installation procedures for optical fibers in steel-concrete composites and investigate the response of the optical fibers during a fire. For brevity, only one representative slab is presented in this paper. The specimen was a reinforced concrete slab supported on two W5×19 steel beams as depicted in Fig. 1(a). Composite action between the concrete slab and steel beams was achieved using headed steel studs. The concrete slab was 1219 mm long and 914 mm wide. It was cast on 0.9 mm thick, trapezoidal metal decking (Vulcraft 3VLI20[1]). The depth of the concrete slab varied from 83 mm to 159 mm as illustrated in Fig. 1(b). The concrete slab was reinforced with welded wire mesh (6×6 W1.4/W1.4), which has a specified mesh spacing of 150 mm and a wire diameter of 3.4 mm. The headed steel studs (Nelson S3L) had a specified shaft diameter of 19 mm and an effective embedment length of 117 mm. The two W5×19 steel beams were 1,829 mm long and placed in parallel with 610 mm spacing.

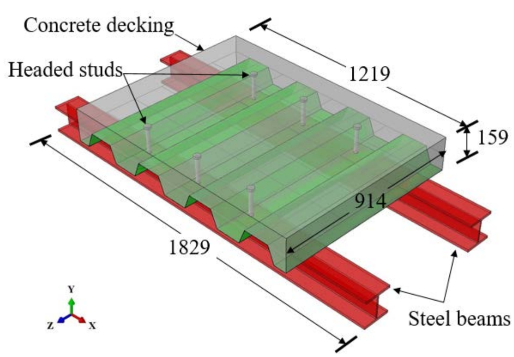

(a)

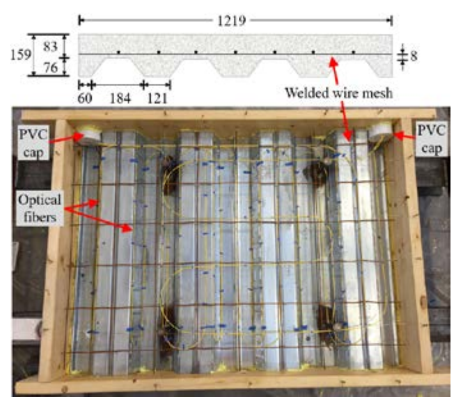

(b)

Fig. 1. Steel-concrete composite slab specimens: (a) isometric rendering, and (b) cross-sectional and top views (all units in mm).

[1] Certain commercial products are identified in this paper to specify the materials used and the procedures employed. In no case does such identification imply endorsement or recommendation by the National Institute of Standards and Technology, nor does it indicate that the products are necessarily the best available for the purpose.

2.2 Material Properties

The design concrete mix used in this study was 0.193: 0.105: 0.315: 1.0: 1.136 by weight for water: fly ash: Type I Portland cement: river sand: expanded slate lightweight aggregate (LWA). This mix corresponded to a water-to-binder ratio of 0.46, a binder-to-sand ratio of 0.42, and a sand-to-LWA ratio of 0.88. The river sand had a diameter up to 4.75 mm. The LWA used had low water-retention characteristics and high desorption (Meng et al. 2017) to expedite the curing of the specimens. A polycarboxylate-based high-range water reducer was used to improve flowability of the concrete. Polypropylene microfibers (FRC MONO-150) with a nominal diameter of 38 μm and lengths between 13 mm and 19 mm were added to the mix at a dosage of 2.37 kg/m^3 of concrete to reduce thermal spalling.

During composite specimen casting, ten standard cylinders measuring about 102 mm in diameter and 203 mm in height were prepared for concrete material testing. Five cylinders were tested and analyzed to determine the average ± standard deviation of each concrete property. Specifically, the measured concrete density was (2,070 ± 80) kg/m^3 at 28 days. The compressive strength of concrete was (38 ± 3) MPa at 28 days and (41 ± 3) MPa at 56 days, which were determined in accordance with the American Society for Testing and Materials standard ASTM C39/C39M. A relative humidity sensor (Vaisala HM40S RH Probe) was inserted into each concrete slab from its top to measure the internal relative humidity of concrete at a depth of 90 mm.

2.3 Instrumentation and Test Setup

The specimen was instrumented with three distributed fiber optic sensors as shown in Fig. 2. The result from one sensor is reported in this paper. The sensor was laid on top of the metal decking and ran parallel to the flutes of the metal decking. The curved portions of the fiber optic sensor were labeled as B1 to B14. The distributed sensor entered the concrete from a polyvinyl chloride (PVC) cap at Point A. The cap measured 100 mm in diameter and was used to protect the fibers from damage during concrete casting. The optical fiber had a buffer (diameter: 900 μm), an outer coating (outer diameter: 242 μm), an inner coating (outer diameter: 190 μm), a glass cladding (outer diameter: 125 μm), and a glass core (diameter: 8.2 μm) (Huang et al. 2013). The optical fiber was free to slide in the sheath so that it was approximately free of axial strain. Thus, the distributed sensor can be used to measure temperature changes (Bao et al. 2017).

Each composite specimen was also instrumented with six glass-sheathed, bare bead, K-type thermocouples (24-gauge wire). The thermocouples were designated TC1 to TC6: TC1 on the top surface of the metal decking in the center of the specimen, TC2 on the welded wire mesh in the center of the specimen, TC3 on the welded wire mesh 305 mm away from the mid-span, TC4 on a headed stud 300 mm away from the mid-span, and TC5 and TC6 peened into a small drill hole (1.5 mm) in the center bottom flanges of the steel beams. An Inconel-shielded thermocouple located 25 mm below the metal decking at the center of the compartment was used to measure the gas temperature below the concrete deck. The thermocouples have a manufacturer-specified temperature standard limit of error of 2.2 °C or 0.75 % (whichever value is greater) over a range of 0 °C to 1250 °C. The total expanded uncertainties for the material temperature and gas temperature measurements are ±6.2 % and ±14.7 % of the reading, respectively. The total expanded uncertainty for the burner heat release rate is less than ±2.4 % (Bundy et al 2007). Data from the fuel delivery system and thermocouples were recorded at a rate of 1 Hz.

Fire tests were conducted in the National Fire Research Laboratory at the National Institute of Standards and Technology (NIST). The test setup was not intended to represent a particular structure, but rather to investigate the performance of fiber optic sensors in a typical steel-concrete composite structure. Fig. 3 depicts the test setup located under a 6 m × 6 m (plan) exhaust hood (not shown in photo). The flame source was a natural gas diffusion burner measuring 530 mm × 530 mm × 200 mm (length × width × height). Natural gas entered the burner near the bottom, filled the burner cavity and percolated through a gravel layer to distribute the gas. The burners were manually regulated using a needle valve on the gas supply line. A skirt constructed of cold-formed steel framing and cement board lined with thermal ceramic fiber blanket partially enclosed the space above the burner to trap hot gases beneath the specimen. The skirt was open at the bottom, creating the compartment fire dynamics depicted in Fig. 4(a). The heated 'compartment' created by the skirt was approximately 1220 mm × 920 mm × 30 mm (length × width × height). Each beam was simply-supported at a clear-span of 1530 mm on four supports made of stacked concrete masonry units (CMU). The supports were wrapped with 25-mm thick thermal ceramic blankets for additional thermal protection. Each specimen was subjected to four fire sizes. No mechanical loading beyond the specimen self-weight was applied. The magnitude of the fire was controlled through the burner's calculated heat release rate (HRR). The HRR was held approximately constant at four target levels: 50 kW, 100 kW, 150 kW, and 200 kW. Each of the first three levels was maintained for 2 min, and the last level (200 kW) was maintained for 210 min, before the fire was extinguished. In total, the specimen was heated for 216 min (3 h and 36 min). The compartment upper layer gas temperature corresponding to the HRR of 200 kW was sustained at about 900 ºC.

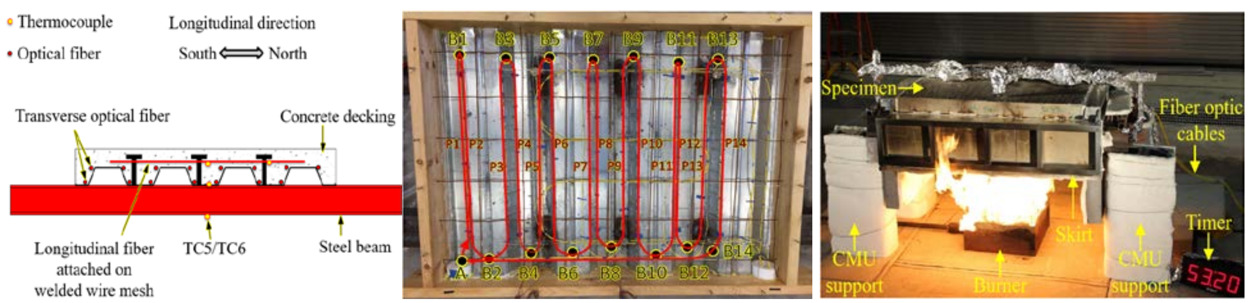

(a) (b) (c)

Fig. 2. Instrumentation layout: (a) overview, (b) top view of the distributed sensor, (c) test set-up.

3. Results and Discussion

Temperature distributions along the distributed sensor are plotted in Fig. 3. The time is relative to burner ignition. The horizontal axis represents the distance along the distributed sensor. The vertical axis represents the measured temperature, which was obtained from the Brillouin frequency shift measured by the distributed sensor and the frequency-temperature calibration curve (Bao et al. 2015). Temperature increases with time as expected during the heating phase of the experiment. The peaks in the temperature distributions in Fig. 3 are marked as 'Pn', where 'n' indicates the location of the peak corresponding to the positions shown Fig. 2(b). The first 14 peaks are marked as P1 to P14, which are along the centerline of the specimen. The fact that the peaks occurred along the centerline suggests that: (1) the gas temperature and radiative heat flux was lower near the edges of the test setup; (2) there was more heat loss from the specimen to the surrounding environment at its edges; and (3) the steel beams near the edges provided heat sink for the concrete slab. The temperature variation transversely across the specimen is significant; over 600 °C variation for fiber section B7 to B8. This spatial variation would commonly be neglected in thermo-mechanical analysis where it is typically assumed that gas temperature and heat flux below the slab is uniform. P8 and P9 exhibited the highest temperatures directly above the burner. Overall, the temperatures at P1, P4, P5, P8, P9, P12, and P13 are higher (on the order of 200 °C to 400 °C) than the temperatures at P2, P3, P6, P7, P10, P11, and P14, suggesting that the lower flanges of the concrete slab were subjected to more intense thermal conditions than the higher flanges because they were closer to the burner. The peaks after P14 are marked by the locations of the curved portions of the distributed sensor. For instance, the peak B10, which is a peak after P14, corresponds to the distributed sensor near B10.

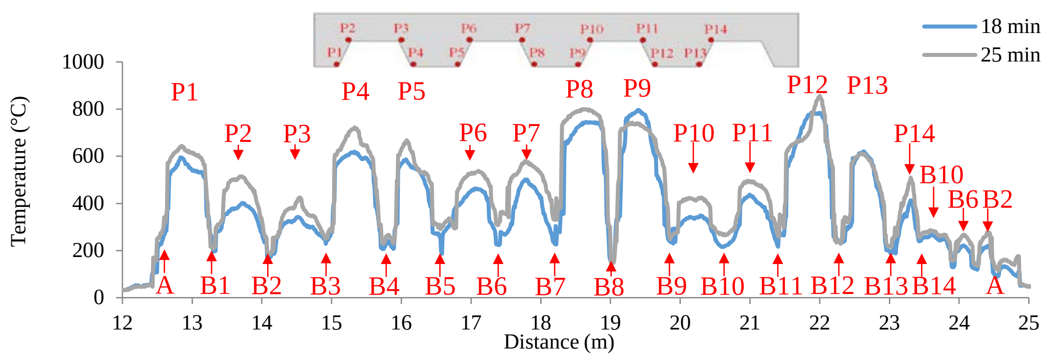

Fig. 3. Temperature distributions measured from the distributed fiber optic sensor.

4. Conclusions

In this study, pulse pre-pumped Brillouin optical time domain analysis (PPP-BOTDA) was used to measure temperatures in distributed fiber optic sensors installed in a steel-concrete composite slab specimen exposed to fire. The limited set of data demonstrated that the investigated commercially-available, polymer-sheathed optical fiber survived the concrete casting process. Material temperatures higher than 900 °C were measured at the interface between the concrete and the metal deck with adequate sensitivity and accuracy for typical structural engineering applications.

The measured temperatures from a distributed fiber optic sensor indicate highly non-uniform temperature distribution in the composite slab, which is often neglected in engineering design and analysis. Deploying the distributed fiber optic sensors in large-scale structural fire tests has potential to improve our understanding on the performance of infrastructure in fires and thus fire safety.

Acknowledgements

This work was funded by the National Institute of Standards and Technology (NIST) [grant No. 70NANB13H183]. The authors thank Alana Guzetta of US Concrete and Dale Bentz of NIST for their assistance in the concrete design.

References

Bao, Y., Chen, G. (2015). "Fully-distributed fiber optic sensor for strain measurement at high temperature," *Proc. 10th Int. Workshop Struct. Health. Monit.*, Stanford, CA.

Bao, Y., Chen, G. (2016a). "Temperature-dependent strain and temperature sensitivities of fused silica single mode fiber sensors with pulse pre-pump Brillouin optical time domain analysis," *Mes. Sci. Tech.*, 27(6), 65101–65111.

Bao, Y., Chen, G. (2016b). "High temperature measurement with Brillouin optical time domain analysis," *Opt. Lett.*, 41(14), 3177–3180.

Bao, Y., Chen, Y., Hoehler, S.M., Smith, M.C., Bundy, M., Chen, G. (2016). "Experimental analysis of steel beams subjected to fire enhanced by Brillouin scattering-based fiber optic sensor data," *J. Struct. Eng.*, 143(1), 04016143.

Bao, Y., Hoehler, M.S., Smith, C.M., Bundy, M., Chen, G. (2017). "Temperature measurement and damage detection in concrete beams exposed to fire using PPP-BOTDA based fiber optic sensors," *Smart Mater. Struct.*, 26(10), 105034.

Bertola, V., Cafaro, E. (2009). "Deterministic-stochastic approach to compartment fire modeling," *Proc. R. Soc. London, Ser. A*, 465, 1029–1041.

Bundy, M., Hamins, A., Johnsson, E.L., Kim, S.C., Ko, G.H., Lenhert, D.B. (2007). "Measurements of heat and combustion products in reduced-scale ventilation-limited compartment fires," *NIST Technical Note*, 1483.

Huang, Y., Fang, X., Zhou, Z., Chen, G., Xiao, H. (2013). "Large-strain optical fiber sensing and real-time FEM updating of steel structures under the high temperature effect," *Smart Mater. Struct.*, 22(1), doi:10.1088/0964-1726/22/1/015016.

Jeffers, A.E., Sotelino, E.D. (2012). "An efficient fiber element approach for the thermo-structural simulation of non-uniformly heated frames," Fire Safety J., 51, 18–26.

Li, G., Zhang, C. (2012). "Simple approach for calculating maximum temperature of insulated steel members in natural-fires," *J. Constr. Steel Res.*, 71, 104–110.

Li, X., Wang, J., Bao, Y., Chen, G. (2017a) "Cyclic behavior of damaged reinforced concrete columns repaired with environment-friendly fiber-reinforced cementitious composites," *Eng. Struct.*, 136, 26–35.

Li, X., Bao, Y., Xue, N., Chen, G. (2017b). "Bond strength of steel bars embedded in high-performance fiber-reinforced cementitious composite before and after exposure to elevated temperatures," *Fire Safety J.*, 92, 98–106.

Li, X., Bao, Y., Wu, L., Yan, Q., Ma, H., Chen, G., Zhang, H. (2017c). "Thermal and mechanical properties of high-performance fiber-reinforced cementitious composites after exposure to high temperatures," *Constr. Build. Mater.*, 157, 829–838.

McAllister, T., Luecke, W., Iadicola, M., Bundy, M. (2012). "Measurement of temperature, displacement, and strain in structural components subject to fire effects: concepts and candidate approaches," *NIST Technical Note*, 1768, 73.

Meng, W., Khayat, K.H. (2017). "Effects of saturated lightweight sand content on key characteristics of ultra-high-performance concrete," *Cem. Concr. Res.*, (101), 46–54.